Droplet Spectra Broadening in Cumulus Clouds. Part II: Microscale Droplet Concentration Heterogeneities

LAURE CHAUMAT

Météo-France, CNRM/GMEI, Toulouse, France

JEAN-LOUIS BRENGUIER

Météo-France, CNRM/GMEI, Toulouse, France, and NCAR/ATD+MMM, Boulder, Colorado

(Manuscript received 12 February 1999, in final form 5 July 2000)

ABSTRACT

Cloud samples of narrow spectra observed in adiabatic cores of cumulus clouds are selected and the droplet spatial distribution is examined in order to document microscale heterogeneities of the droplet concentration. Counting statistics and the Fishing test are applied and compared to the properties of a random spatial distribution, that is, to Poisson statistics. These tests suggest that microscale heterogeneities of the concentration are not significant in adiabatic cores. A conceptual model is then developed to estimate the lifetime that would be required for the observed heterogeneities to generate the observed spectra broadening. The model implies that the lifetime of the heterogeneities should reach unrealistic values to significantly contribute to the observed broadening. The statistical properties of direct numerical simulations of the droplet inertial coupling with turbulence are then compared to the properties of the actual samples. It appears that the properties of the actual samples are closer to the Poisson reference than those of the fields generated by the models. It is concluded that the microscale observations of the droplet spatial distribution in adiabatic cores do not support the hypothesis that inertial coupling is a significant source of spectra broadening.

1. Introduction

This second paper of the series dedicated to the experimental study of droplet spectra broadening (DSB) in cumulus clouds is focused on the potential effects of microscale droplet concentration heterogeneities on condensational droplet growth. DSB refers to droplet spectral shapes broader than predicted with the adiabatic model of ascending parcel, where it is implicitly assumed that the supersaturation field is uniform. Equation (2) in the first paper of the series, Brenguier and Chaumat (2001, hereafter referred to as Part I), shows that, in the adiabatic prediction, the droplet surface distribution is translated along the ϕ^2 scale, while the shape of the spectrum remains unchanged. By using the droplet surface distribution instead of the size distribution, spectral shapes observed at various levels in a convective cloud can be directly compared to a reference spectrum at cloud base, either calculated with a model of cloud condensation nuclei (CCN) activation, or measured slightly above cloud base. The key parameter in the procedure is the Lagrangian integral of the ratio of supersaturation to vertical velocity along the adiabatic parcel trajectory, from the activation level to the observation level. It is referred to here as β^2. If the observed and the reference spectra are comparable, the translation β^2 required to superimpose the observed spectrum with the reference one provides information about the amount of condensate from the cloud base to the observation level [Eq. (3) in Part I]. If the observed spectrum is broader than the reference, Eq. (4) in Part I shows how to characterize broadening by the β^2 probability density function (PDF), $\Psi(\beta^2)$. It is interesting to note here that local fluctuations of the supersaturation relative to each droplet are not sufficient for generating DSB. It is in fact necessary that those fluctuations result in a diversity of the β^2 values for the droplets composing the observed spectrum.

Physical reasons for such a diversity are numerous in a convective cloud as soon as a spectrum is observed far enough from the cloud base. Observations are made by counting and sizing particles along the track of an instrumented aircraft. As thousands of particles are needed to build a significant spectrum, the spectrum characterization with a droplet spectrometer is limited to a spatial resolution of the order of 10 m at the best, though smaller-scale characterization can be obtained

Corresponding author address: Jean-Louis Brenguier, Météo-France, Centre National de Recherches Meteorologiques, GMEI/MNP, 42 av. Coriolis, 31057 Toulouse Cedex 01, France.
E-mail: jlb@meteo.fr

by Bayesian estimation (Pawlowska et al. 1997). It can be hardly assumed that all the droplets observed at such a scale have followed similar trajectories so that their integrals of the ratio of supersaturation to vertical velocity are identical. The turbulence originating from the convective motion contributes to mixing of parcels following different trajectories and experiencing different rates of condensational growth. In particular, some cloud volumes are exposed to mixing with air entrained from the drier cloud environment. Their droplets can be partly or even totally evaporated during the process. Besides evaporation, when an entrained clear air parcel is forced to rise in the convective core, additional CCN can be activated, producing small droplets. Partial droplet evaporation and secondary CCN activation are thus reasonable explanations to account for the observation of small droplets in the upper levels of a convective cloud. However it must be remembered that the largest value of liquid water content (LWC) at a certain altitude is produced by adiabatic lifting from the cloud base. It is referred to as the adiabatic LWC. Mixing of parcels originating from levels higher than the cloud base always result in subadiabatic LWC. Therefore the ratio of the observed LWC to the adiabatic value calculated at the observation level can be used as an indication that the observed parcel contains air originating from levels higher than the cloud base.

Variability of β^2 can also be produced by mixing of adiabatic parcels originating from the cloud base, if their values of total droplet number concentration are different. For the same amount of condensate, the β^2 value increases when the number concentration decreases. To simulate DSB, one can thus imagine that cloudy parcels with different values of droplet number concentration are formed at the cloud base, lifted separately to the observation level, and then mixed at the scale of the observation (10 m). In such a scenario the observed LWC value is equal to the adiabatic LWC, but the observed spectrum is broader than the adiabatic reference. Such a simplistic concept is not supported by the observations since anticorrelations between droplet sizes and number concentration have not been reported in the literature. However, such entities could have a lifetime so short that they are not detectable with an instrumented aircraft, yet contributing to some DSB.

It is thus obvious that turbulence, entrainment, and mixing are sources of DSB in convective clouds, though it is not clear yet if they are capable of producing superadiabatic droplet growth (see Part I, section 1c for the definition of superadiabaticity). This point will be addressed in Part III (manuscript in preparation) of the series. However along these concepts, it has been assumed that droplets are driven by air motion and that they behave like passive tracers of the turbulence. This is usually true as droplets are characterized by a small Stokes number, but high Reynolds number turbulence in convective clouds is also characterized by huge acceleration spikes, where even small droplets cannot be considered as passive tracers. Following the work of Cooper (1989) and Srivastava (1989) a new concept has been recently introduced (Shaw et al. 1998; Vaillancourt 1998; Vaillancourt et al. 1998; Vaillancourt and Yau 2000) that is based on the coupling between turbulence and droplet inertia to generate microscale heterogeneities of the droplet spatial distribution and consequently some broadening of the size distributions. This paper is dedicated to the analysis of the droplet spatial distribution for an experimental validation of these new concepts.

2. Methodology

As discussed by Cooper (1989) and Srivastava (1989) the local values of supersaturation, at the scale of the droplet environment, are determined by the three-dimensional fields of temperature, water vapor mixing ratio, and the individual positions and sizes of the neighboring droplets. Current calculations, such as done in adiabatic models, are based on the assumption that droplets are randomly distributed in space so that the supersaturation field is uniform. If for some reason there are heterogeneities in the droplet concentration, the supersaturation field is no longer uniform, with values lower than the mean in regions of high concentration and inversely in regions of low droplet concentration. Droplets in the most populated regions are thus growing less than isolated droplets. However, it must also be mentioned that the response of the supersaturation field to the droplet spatial distribution is not instantaneous. The supersaturation field is the result of a combination of the temperature and water vapor mixing ratio, both scalars that are driven by molecular and turbulent diffusion. For concentration heterogeneities to have a significant effect on droplet growth, it is thus also necessary for those heterogeneities to last long enough for the supersaturation to adjust to the droplet spatial configuration [see Vaillancourt and Yau (2000) and Vaillancourt et al. (2001) for the characteristic timescales of these processes]. It is also necessary for those heterogeneities to last long enough for some droplets to experience values of condensational growth very different from the average. This is reflected in our method by the width of the $\psi(\beta^2)$ distribution.

It is presently not possible to precisely assess the effects of microscale heterogeneities on DSB, neither experimentally, nor with a numerical model. Temperature and water vapor mixing ratio cannot be measured in clouds at the microscale. Airborne instruments are limited to resolution scales of the order of a few meters and their performances are significantly affected in clouds by droplet impacts. Besides an instrumented aircraft crossing a cloud at 100 m s^{-1} provides an instantaneous picture of the cloud properties and it cannot document the time evolution of individual droplets. Recent improvements of the Forward Scattering Spectrometer Probe (FSSP) particle droplet counter offer new

opportunities to characterize the droplet spatial distribution, but this is still an instantaneous picture and there is no way to get information about the characteristic correlation time of the observed structures from in situ measurements.

The complete numerical simulation of microscale fluctuations of supersaturation and of their effect on condensational droplet growth would require explicit description of the droplet motions and of the temperature and humidity fields, down to the scale of the droplets. This is far beyond the capability of the present computers and approximations must be made. In Vaillancourt (1998) direct numerical simulation (DNS) is performed, but the corresponding Reynolds number is lower than the typical values encountered in cumulus clouds. High-amplitude fluid accelerations are thus largely absent from the simulated turbulence. Turbulent diffusion of heat and water vapor is also limited to the scale of the model boxes. In contrast, Shaw et al. (1998) formulate a conceptual model in order to explore possible effects of high Reynolds number turbulence on droplet growth but they do not simulate explicitly the concentration heterogeneities from which the conceptual model is derived.

The numerical models are thus capable of simulating the growth history of individual droplets but they do not reproduce precisely the actual heterogeneities at the microscale, while in situ data can provide information about the instantaneous microscale spatial distribution of the droplets but they are not suited for a Lagrangian approach of their condensational growth. Therefore our methodology aims at combining both sets of information by identifying specific features of the numerical simulations that can be verified with in situ measurements. It proceeds in three steps: in sections 3 and 4 statistical tests will be defined to characterize the properties of the droplet spatial distribution and integral radius, respectively, from the measured series of droplet counts with the droplet spectrometer. A conceptual model of droplet growth will then be used in section 5 to get estimates of the characteristic correlation time that would be required for the observed heterogeneities to generate the observed DSB. Finally, the observed properties of the droplet spatial distribution will be compared in section 6 to those simulated by DNS, in order to assess the realism of those simulations. Since Vaillancourt's DNS simulates the droplet spatial distribution, the observations will be directly compared to the simulations, which will be hereafter referred to as PV. This is not possible with the Shaw et al. conceptual model, which does not simulate a droplet field. However, Shaw et al. reference [Fig. 1b in Shaw et al. (1998)] a DNS of turbulence to illustrate the phenomenon of preferential concentration. This simulation was done with parameters (particle Stokes number, dissipation rate, etc.) very different from those typically found in clouds, and it will be used here as an example of the maximum possible preferential concentration achievable at low Reynolds number. It will be hereafter referred to as RS.

The selection of the cloud sections to examine is not trivial. The measurements performed during the Small Cumulus Microphysics Study (SCMS) show extended regions of broad droplet spectra with high fluctuations of the droplet concentration and LWC (Fig. 2 in Part I). Sharp interfaces between regions of clear air and regions of dense cloud are also observed (Brenguier 1993). These regions are obviously affected by mixing with dry air from the environment and droplet evaporation is active. When examining such cloud samples it will not be possible to distinguish between heterogeneities produced by mixing and those related to inertial effects. Our approach thus proceeds a contrario: *if microscale inertial coupling had a significant contribution to DSB, it should not be likely to observe narrow spectra in regions that are not affected by mixing processes.* In Part I, cloud samples with narrow spectra have been selected in the SCMS dataset. It has been shown that they correspond to slightly subadiabatic values of LWC; that is, they are not strongly affected by mixing with the environmental dry air. The same cloud samples will thus be used here to examine the effects of microscale heterogeneities. A priori, heterogeneities occur at all scales from the cloud size to the Kolmogorov microscale (mm). Our analysis shall therefore consider this whole range, from the scale of the selected cloud sections to the millimeter scale. The concept of spatial scale is however dependent upon the sampling technique. A droplet counter is installed on an aircraft flying through the clouds. The counter has a fixed sampling cross section and the droplet arrival times through that section are measured. The volume of air swept by the probe during a sampling period T is equivalent to a long tube with a section of the order of 2.5 mm^2 (the counter's sampling cross section S_t) and a length equal to $L = v_a T$, where $v_a \approx 90$ m s^{-1} is the aircraft speed. Various scales can be explored by changing the sampling period. Such a procedure can thus be considered as a one-dimensional sampling of the three-dimensional droplet field.

The observed counting statistics are then compared to a reference, namely, the Poisson process, that describes counting of a random field of particles. The objective here is to identify deviations from this idealized model that would significantly contribute to DSB. However deviations from the Poisson reference will obviously be detected in actual data for the two following reasons:

1) Cloud samples are not infinite: the samples of narrow spectra that have been selected in Part I of this series are limited to a few seconds of flight. Each sample will be further subdivided into numerous adjacent subsamples for exploring the various scales. As the scale increases, the length of the sample being fixed, the number of independent subsamples decreases and the statistics are less significant. This limitation will

be accounted for in the next section by using confidence levels based on the number of independent subsamples.
2) The droplet spatial distribution cannot be perfectly random at all scales because of its connection with the partly coherent dynamical field.

Various statistical tests can be used, some being very sensitive to deviations from Poisson. Therefore it is not sufficient to demonstrate that actual samples do not exhibit pure Poisson statistics. It is also necessary to evaluate the effects on DSB of the observed deviations from the Poisson statistics.

3. Counting statistics

The measurements analyzed here have been performed with the Fast-FSSP (Brenguier et al. 1998), an improved version of the standard FSSP (manufactured by Particle Measuring Systems, Boulder, Colorado) used during the SCMS-95 experiment (see details in Part I). This device detects and sizes droplets in the diameter range from 1 to 40 μm. The pulse amplitude, pulse duration, and time interval between detections are recorded for each detection. Pulse duration and time interval are counted with a 16-MHz clock, that is, a spatial resolution of 8 μm, along the aircraft track. That allows us to reconstruct the complete series of droplet arrivals in the probe's sampling volume. Measurements of the droplet sizes are considered reliable only when the counted particle crosses the central portion of the sampling section S_t, also called the depth of field (DOF), whose area $S_{\rm dof}$ is about 0.13 mm^2.

For the evaluation of the statistics of the droplet counting and of the integral diameter, only the detections in the DOF sampling section of the probe are considered. The same 50 cloud samples as in Part I are considered here. The mean concentration $\overline{C}$ is then calculated over the selected cloud sample, as $N_{\rm dof}/V_{\rm dof}$, where $N_{\rm dof}$ is the total number of DOF counts over the sample and $V_{\rm dof}$ is the DOF volume swept by the probe along the sample. Here $V_{\rm dof} = S_{\rm dof} v_a T_t$, where T_t is the total duration of the sample. In order to examine various scales, the sample is further subdivided into smaller subsamples of duration $T = T_t/n_t$, where n_t is the number of subsamples. Similarly the volume of air in each subsample is $V = V_{\rm dof}/n_t$ (the aircraft speed is constant over a short period of time) and the expected droplet concentration within a subsample is assumed to be equal to the mean over the whole sample. It follows that the expected number of counts $\overline{N}$ in a subsample is given by $\overline{N} = N_{\rm dof}/n_t = \overline{C}V$. The corresponding length scale is $L = v_a T$.

a. Poisson statistics

If the droplets are randomly distributed at the scale L, within the n_t subsamples, the probability of counting N particles is given by Poisson as

$$P(N|\overline{N}) = \frac{\overline{N}^N}{N!} e^{-\overline{N}}. \quad (1)$$

When the number of samples tends to infinity the variance of the distribution of N is $\sigma^2(N) = \overline{N}$. When the number of samples n_t is finite, the measured variance $\sigma_m^2(N)$ is likely to deviate from its expected value. It is possible to check the Poisson hypothesis with a limited number of samples by using the clustering index, CI(L) [see Eq. (5.18), p. 78, in Barlow (1989)], or the Fishing test $F(L)$ (Baker 1992). They are, respectively, defined as

$$\mathrm{CI}(L) = \frac{\sigma_m^2(N)}{\overline{N}} - 1 \qquad F(L) \equiv \frac{\mathrm{CI}(L)}{\sigma(n_t)}, \quad (2)$$

where $\sigma(n_t) \approx [2/(n_t - 1)]^{1/2}$.

If the droplet spatial distribution follows Poisson statistics, F, calculated with a significant number of samples, $n_t\overline{N} > 100$ (Baker 1992), has a probability of 68% to be within the range ± 1, and a probability of 99.7% to be within the range ± 3.

b. Observations

Figures 1 and 2 show examples of the counting statistics for two selected cloud samples. The first one has a total length of 144 m and it has been divided into subsamples of length between 2 and 108 mm, as indicated in the figure. The corresponding values of $\overline{N}$ are also reported. The second one has a total length of 54 m and it has been divided into subsamples of lengths between 2 and 88 mm. The total number concentrations are $\overline{C} = 329$ cm^{-3} and 246 cm^{-3}, respectively.

Both examples exhibit remarkable agreement between the observed distributions and the Poisson prediction, even at large scale, where the spurious variations of the observed distributions are due to the reduced number of samples. This preliminary test suggests that the droplets are randomly distributed in adiabatic cores.

The fishing test provides a more synthetic view of the scale dependence of the counting statistics. Figures 3 shows $F(L)$ for four selected cloud samples, in the range of subsample lengths from 0.001 to 30 m in 3a, and from 0.001 to 0.1 m in 3b. Here $F(L)$ exceeds its expected range of variability (± 3) at both the very small and the very large scales. Large-scale variability simply reflects large-scale turbulent fluctuations of the concentration that are not relevant in a study of the inertial coupling. At small scale, shorter than 5 mm, the variability is more difficult to interpret and part of it can be due to a bias in the measurements of pulse durations and interarrival times.

4. Statistics of the integral diameter

The analysis of the droplet counts, presented in the previous section, shows that the observed statistics of counting are close to the idealized Poisson statistics. How-

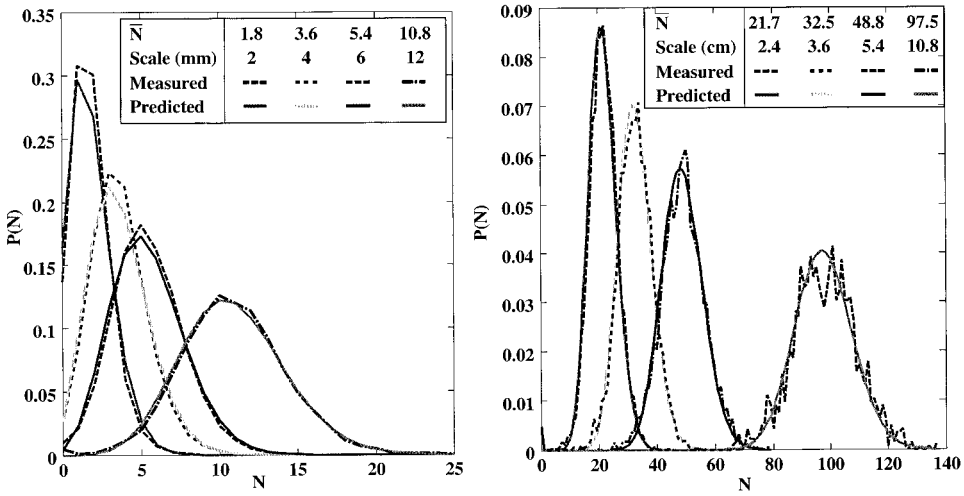

FIG. 1. Probability distribution of the number of counts in actual subsamples (dashed lines), compared to the Poisson distribution (solid lines), for various values of subsample sizes, i.e., of $\overline{N}$. The corresponding spatial scale is indicated in the legend. SCMS sample, at 1542:18.6 UTC 10 Aug 1995 (duration: 1.6 s): $z = 2188$ m, $C = 329$ cm^{-3}, $\overline{\phi} = 25.7$ μm.

ever the key parameter in the condensation process is not specifically the local droplet concentration, but rather the sum of the droplet sizes, also referred to as the integral diameter. It is defined in a volume of air V as

$$I = \frac{1}{V}\sum_{i=1}^{N} \phi_i, \tag{3}$$

where i corresponds to the individual droplets and N is the number of droplets in the volume V.

This parameter can be estimated directly from the measurements of the droplet sizes with the Fast-FSSP. The estimations will be used here to validate a simple model of the integral diameter statistics, which is required for the development of our conceptual model of DSB.

a. First- and second-order statistics

The Poisson process generally refers to a point process of random events. When the points are associated to an auxiliary variable, also referred to as a mark (the droplet diameter ϕ in this case), the process is rather called a marked point process [see section 3 in Snyder (1975)]. The parameter of interest in the condensation process, namely, the integral diameter (I), corresponds to the sum of the marks in each sample. Here N is the number of events in a sample, $\overline{N}$ is its expected value (the parameter of the Poisson process), ϕ is the mark of the points, and $\overline{\phi}$ is its expected value. According to Snyder [Eqs. (3.19) and (3.20)], the mean and the variance of I, for a Poisson process, expresses as

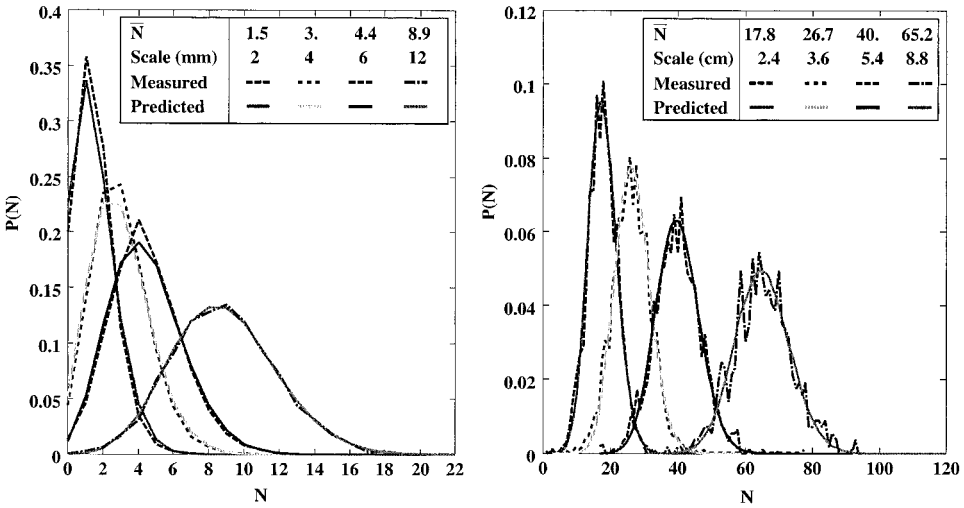

FIG. 2. Similar to Fig. 1 for another SCMS sample, at 1602:22.6 UTC 4 Aug 1995 (duration 0.6 s): $z = 2092$ m, $C = 246$ cm^{-3}, $\overline{\phi} = 27.5$ μm.

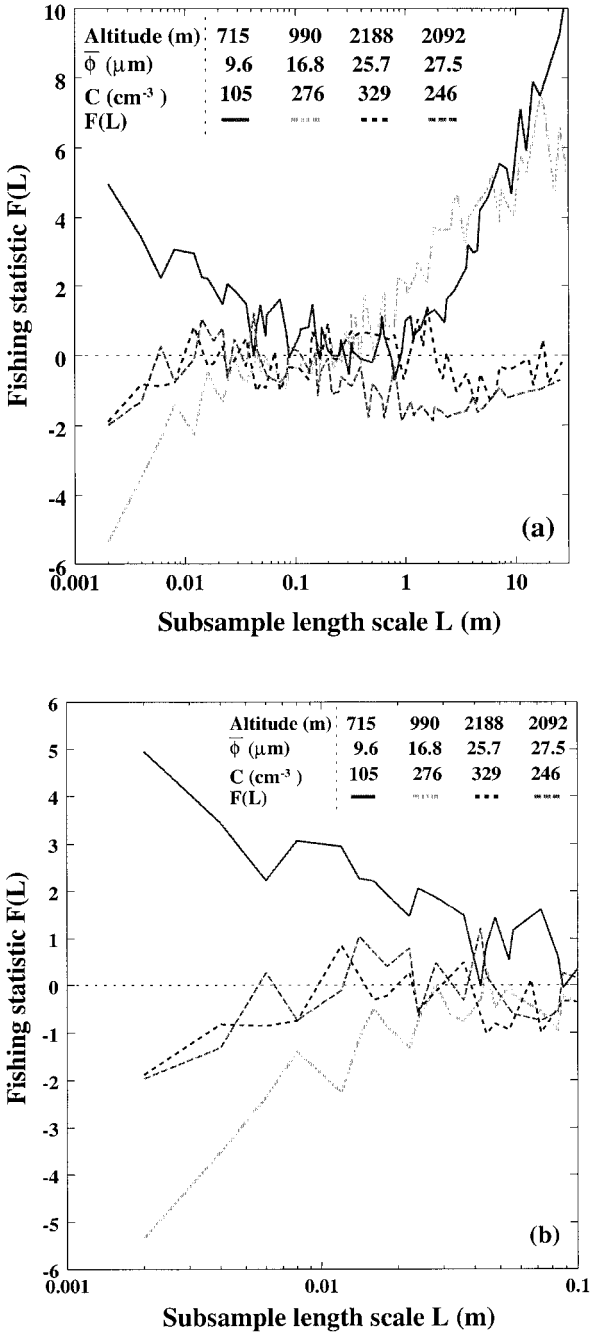

FIG. 3. Fishing test for four SCMS cloud samples, whose characteristics are indicated in the legend. Sample 1: 1625:30.3 UTC 10 Aug 1995 (duration 0.8 s), sample 2 same as in Fig. 5, sample 3 same as in Fig. 1, sample 4 same as in Fig. 2. The length scale ranges (a) from 0.001 to 30 m and (b) from 0.001 to 0.1 m.

$$V\overline{I} = \overline{\phi}\,\overline{N} \quad \text{and} \quad V^2\sigma^2(I) = \overline{\phi^2}\,\overline{N}, \tag{4}$$

that is,

$$V^2\sigma^2(I) = [\sigma^2(\phi) + \overline{\phi}^2]\overline{N}. \tag{5}$$

As shown in Part I, the droplet spectra in the selected cloud samples are narrow and $\sigma^2(\phi) \ll \overline{\phi}^2$. Examples are given in Table 1. It follows that

$$V^2\sigma^2(I) \approx \overline{N}\,\overline{\phi}^2 = \sigma^2(N\overline{\phi}). \tag{6}$$

This result suggests that the statistics of the integral diameter can be reduced to the statistics of counting, as if all the droplets had the same diameter $\overline{\phi}$.

TABLE 1. Characteristics of the four selected SCMS cloud samples shown in Fig. 3.

Sample	Date	Altitude (m)	$\overline{\phi}$ (μm)	$\sigma^2(\phi)$ (μm^2)	C (cm^{-3})
1	10 Aug	715	9.61	2.05	105
2	10 Aug	990	16.81	3.73	276
3	10 Aug	2188	25.72	7.69	329
4	04 Aug	2092	27.86	13.29	246

b. Observations

In order to validate the above statement, the statistics of the integral diameter have been calculated at various scales, the same way that the counting statistics have been calculated in the previous section. Figures 4 and 5 show the cumulative frequency distribution of I compared to the statistics of $N\overline{\phi}$ and $N_P\overline{\phi}$, where N is the number of particles actually counted in the subsample, while N_P corresponds to a Poisson distribution with a parameter equal to $\overline{N}$, the mean value over the whole cloud sample. The values of integral diameter have been normalized by the mean value over the whole sample $\overline{I}$, in order to compare the statistics for subsamples of different length scales. The corresponding $\overline{N}$ values are reported in the figures. The cumulative distribution axis is transformed to a normal distribution axis to emphasize the probabilities of small and large values of I.

The figures show good agreement between the observed distributions of the integral diameter and the ones predicted with a Poisson distribution of counts and a mean diameter equal to the measured one. These observations, as well as other examples not shown here, confirm the above statement. In the conceptual model the statistics of the integral diameter will thus be derived from the Poisson statistics as

$$P(I = N\overline{\phi}) = Q(N|\overline{N}), \tag{7}$$

where $P(I)$ is the probability distribution of I and $Q(N|\overline{N})$ is Poisson distributed (1).

5. Conceptual model

a. Model description

The spatial distribution of the droplets is a potential source of variability of the supersaturation, and therefore of DSB. Heterogeneities occur at all scales and their time evolution depends upon the time evolution of the droplet spatial distribution, which generates the supersaturation variability, and upon diffusion of heat and

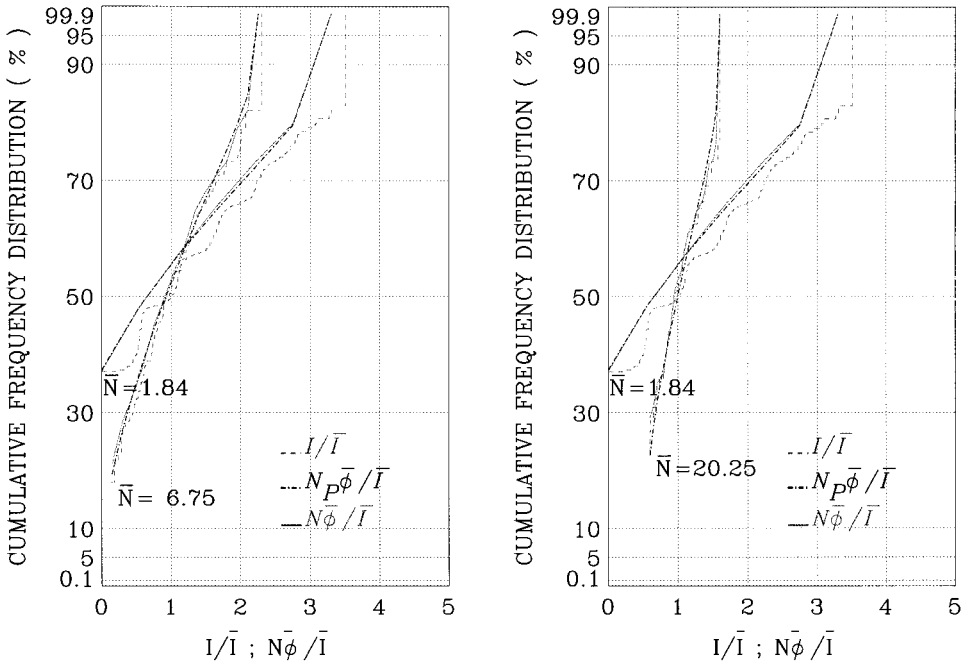

FIG. 4. Cumulative frequency distribution of I compared to the statistics of $N\overline{\phi}$ and $N_P\overline{\phi}$, for three values of $\overline{N}$: (a) 1.84 and 6.75, (b) 1.84 and 20.25. Same cloud sample as in Fig. 2.

water vapor, which tends to reduce the variability. The characterization of the supersaturation statistics, including moments higher than the second order, requires explicit numerical simulation. In a first step, a simplified conceptual model of supersaturation variability and of its effect on DSB is developed. The simplifications are the following:

1) Only one scale is considered at a time. The volume of air in the updraft is divided into boxes of size L

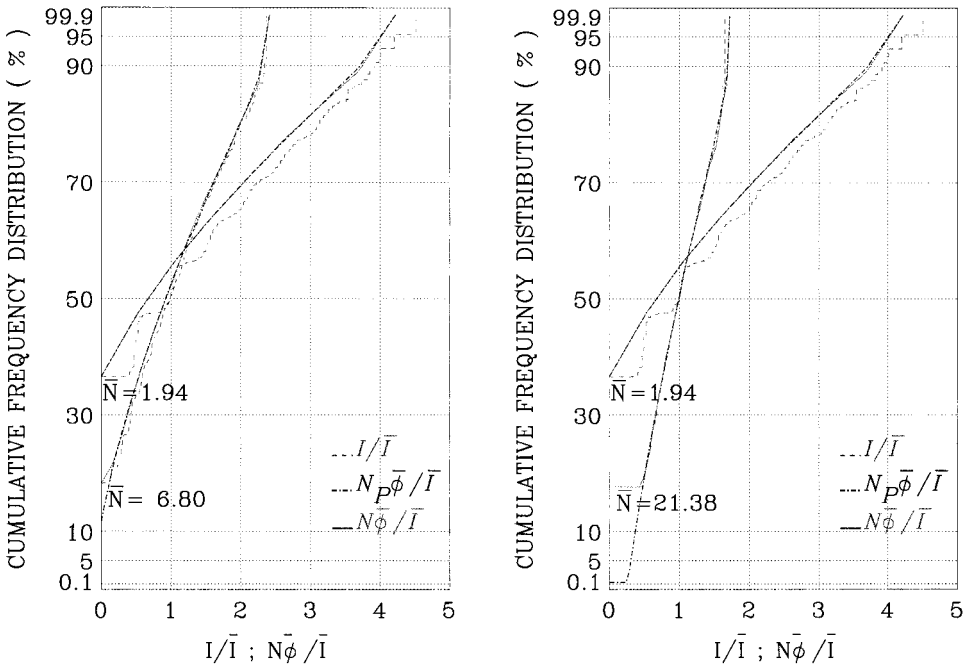

FIG. 5. Same as Fig. 4 for a flight section sampled at 1631:39.2 UTC 10 Aug 1995 (duration 4.1 s): z = 990 m, C = 276 cm^{-3}, $\overline{\phi}$ = 16.81 μm.

(volume V). The number of particles in each box is Poisson distributed and the supersaturation is supposed to be uniform within the box.
2) The effects of heat and water vapor diffusion are neglected between adjacent boxes.
3) The continuous time evolution of the process is replaced by an independent increment process. The droplet distribution and the supersaturation field are frozen during a time Δt. After Δt, the droplets are redistributed randomly, according to a Poisson distribution, and independently from the previous distribution.
4) In each box the supersaturation is instantaneously equal to its quasi-stationary value S_{qs} (Squires 1952),

$$S_{qs} = \frac{Bw}{I}, \tag{8}$$

where B depends only on pressure and temperature.
5) The probability distribution of I is given by Eq. (7) above.

The droplet spectra are represented by the droplet surface distribution $f(\phi^2)$ and DSB is characterized by the β^2 PDF, $\Psi(\beta^2)$. The model starts with an initial spectrum $f(\phi^2, z_0)$, and proceeds with time steps Δt. During that period of time, the parcel is ascending by $\Delta z = w\Delta t$, where w is the updraft vertical speed. According to Eq. (2) in Part I, and the definition of the quasi-stationary supersaturation (8), the β^2 increment in a box during Δt is given by $\Delta\beta^2(N) = 2D\ \Delta z/I(N) = 2D\ \Delta z/N\overline{\phi}$, where $D = AB$ [A and B are the constants in Eq. (1) of Part I and Eq. (8) above, respectively]. The frequency distribution of $\Delta\beta^2$ is thus equivalent to the distribution of $1/N$, with N being Poisson distributed. The next step would be to derive $\overline{\phi}$ from the spectrum and the distribution of $\Delta\beta^2(N)$ from the distribution of N. A faster solution is to calculate the increment in adiabatic liquid water mixing ratio, $\Delta q_A(\Delta z)$, and to derive the corresponding increment, $\Delta\beta_A^2$, as in Eq. (3) of Part I. The values of $\Delta\beta^2(N)$ are then deduced from the adiabatic estimation as $\Delta\beta^2(N) = \Delta\beta_A^2\overline{N}/N$, with a probability distribution identical to the distribution of $N|\overline{N}$ given by Eq. (1). The values of $\Delta\beta^2(N)$, with their respective probabilities $P(\Delta\beta^2)$, are then used to derive the droplet distribution $g(\phi^2, z_{i+1})$ and the β^2 PDF, $\Psi(\beta^2, z_{i+1})$ as:

$$g(\phi^2, z_{i+1}) = \sum_{N=0}^{N=\infty} P(\Delta\beta^2) g(\phi^2 - \Delta\beta^2, z_i), \quad \text{and} \tag{9}$$

$$\Psi(\beta^2, z_{i+1}) = \sum_{N=0}^{N=\infty} \Psi(\beta^2 - \Delta\beta^2, z_i) P(\Delta\beta^2), \tag{10}$$

where $z_{i+1} = z_i + \Delta z$, and $g(\phi^2, z_0) = f(\phi^2, z_0)$. Practically the range of N values in the summation is restricted to values such that $P(N)/P(\overline{N}) > 10^{-4}$.

This model was run for various of the cases described in Part I. Each case is characterized by its initial spectrum $f(\phi^2, z_0)$ measured at a level z_0, slightly above the activation level, and an observed spectrum $g(\phi^2, z)$ measured higher in the cloud at a level z. The procedure described above is thus repeated from z_0 to z and the resulting spectrum at the level z is compared to the observed one. Consistency of the calculation is assessed at each time step by verifying, according to Eq. (4) in Part I, that $g(\phi^2, z_i) = \int_0^\infty \Psi(\beta^2, z_i) f(\phi^2 - \beta^2, z_0)\, d\beta^2$.

The results are mainly dependent upon two parameters, the box volume V, which determines the value of $\overline{N} = \overline{C}V$ and the time step Δt, which also determines the number of altitude steps $n = (z - z_0)/(w\Delta t)$. When the box volume decreases the variability in N increases according to (1). In addition when the time step increases the effects on DSB become more significant according to (9) and (10). In the conceptual model, the time step reflects the autocorrelation time of the supersaturation fluctuations, that is the time needed for a droplet spatial distribution to be renewed by turbulence. It is therefore related to the box volume. In fact it is likely that when the box volume gets smaller, the characteristic time of autocorrelation should also get shorter.

b. Model results

Figure 6 illustrates the results of simulation for the cloud sample shown in Fig. 4a of Part I ($\overline{C} = 225\ \text{cm}^{-3}$). The solid lines represent the initial spectrum (narrow spectrum to the left), and the one observed higher in the cloud (broad spectrum to the right). The model results are displayed by dashed lines, corresponding to three values of the altitude/time increment, 20 m/4 s, 181 m/36 s, and 363m/72s ($w = 5\ \text{m s}^{-1}$). Figure 6a corresponds to a box volume of 0.07 cm^3 ($\overline{N} = 15$), while 6b corresponds to a volume 10 times bigger ($V = 0.7\ \text{cm}^3$, $\overline{N} = 150$).

This figure, as well as other simulations not shown here, suggests that the random spatial distribution of the droplets could contribute to the observed DSB, only if heterogeneities at scales smaller than half of a centimeter ($0.07^{1/3}$) have a characteristic lifetime longer than 40–70 s. When considering that in such convective clouds, the Kolmogorov characteristic time is of the order of 0.04 s, such a condition appears very unlikely.

6. Comparison with DNS

The conceptual model used in the previous section suggests that concentration heterogeneities, with statistical properties similar to the ones observed in cloud regions that are not significantly affected by mixing, are not likely to generate DSB. However, the conceptual model has serious limitations. In particular heat and water vapor diffusion is not treated and individual droplets are not tracked for the calculation of their Lagrangian condensational growth. On the contrary, DNS provides a way of tracking individual droplets. Numerical studies have been recently devoted to the droplet inertial coupling with turbulence to generate concentration het-

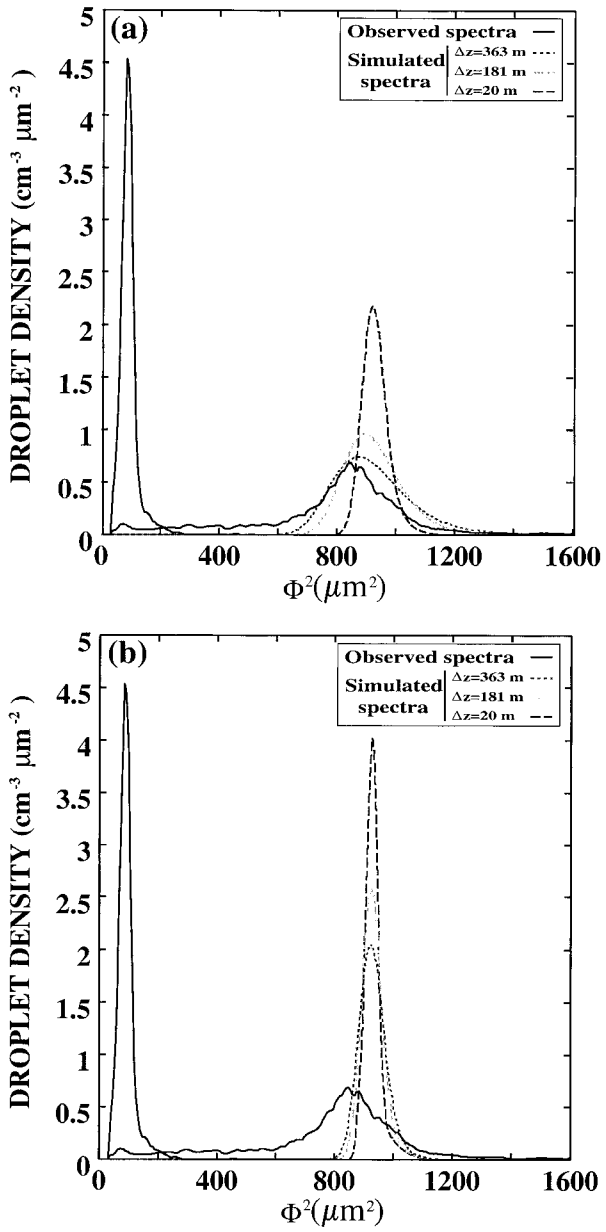

FIG. 6. Examples of simulations with the conceptual model, compared to the cloud sample at 1526:52.6 UTC 10 Aug 1995 (duration 2 s): $\overline{C}$ = 225 cm^{-3}, z = 2170 m. The narrow spectrum on the left is the initial spectrum, at cloud base, and the broad spectrum on the right is the observed one higher in the cloud (solid lines). The simulated spectra are represented by three dashed lines, corresponding to three values of the altitude/time step as indicated in the legend. (a) Box volume of 0.07 cm^3 ($\overline{N}$ = 15). (b) Box volume of 0.7 cm^3 ($\overline{N}$ = 150).

erogeneities, and to their effects on DSB. Such heterogeneities are also referred to as preferential concentration. It is thus relevant to identify properties in the simulations that can be compared to the observations in order to evaluate how the simulation agrees with properties observed in real clouds. In fact this can easily be done when the numerical model simulates a droplet field as in Vaillancourt (1998). It is more difficult to design a test with the conceptual model of Shaw et al. (1998).

The same statistical tests as in section 3 are performed on the simulated fields. Each field is divided into subsamples of volume V and the number N of droplets in each subsample is counted. The expected number of counts is derived from the mean concentration in the simulation $\overline{C}$, as $\overline{N} = V\overline{C}$. The Fishing test is calculated according to (2), where the length scale $L = V^{1/3}$. Two simulations will be used for the comparison: (i) The PV simulation is a 3D nonhydrostatic numerical simulation of turbulence including heat and vapor diffusion, droplet inertia, and sedimentation. The simulated fields are obtained with an eddy dissipation rate ϵ of 160 cm^2 s^{-3} and a Kolmogorov characteristic time τ_η of 0.03 s. All the droplets have a diameter of 40 μm and a Stokes number St = 0.16. The particles are initially randomly distributed with a mean concentration $\overline{C}$ = 50 cm^{-3}. The lifetime of the heterogeneities τ_s is 0.16 s. The size of the domain is 1 dm^3.

The four PV fields correspond to t = 0, 0.16, 0.32, and 1.6 s. At t = 0 s the droplets are randomly distributed in the domain. As time evolves, inertial effects and sedimentation are progressively generating preferential concentration and it is assumed that the simulation has reached a stationary state after 1.6 s of simulation.

(ii) The RS field was provided by Shaw et al. (1998) as an illustration of preferential concentration. It has been generated by a DNS model, with a 64^3 domain containing 64^3 particles with St = 1, and zero fall velocity. By assuming that the smallest resolved spatial scale is of the order of η, we estimate a droplet concentration of $\overline{C}$ = 260 cm^{-3}. Correspondingly, the scaled domain size is 64η, approximately 6 cm.

a. Counting statistics

Figure 7 similar to Fig. 2 shows the counting statistics for the PV initial and final fields. The initial field exhibits distributions very close to the Poisson distribution, even at the largest scale of 1 cm^3 ($\overline{N}$ = 50), for which only 1000 subsamples are available to build the distribution. The final field reflects the effects of droplet inertial coupling and sedimentation. The distributions are significantly broader than the Poisson reference. The comparison with Figs. 1 and 2 reveals that the statistical properties of actual droplet spatial distributions in adiabatic cores are closer to the Poisson reference than to the PV final simulation. In fact the actual distributions do not show deviations from Poisson larger than the PV initial field. It can thus be concluded that the differences between actual counting statistics and Poisson with this test can be mainly attributed to the limited number of samples.

The Fishing test is reported in Fig. 8, similar to Fig. 3b, for the four PV simulations. This test illustrates the increase of the variance of counts when droplet inertial

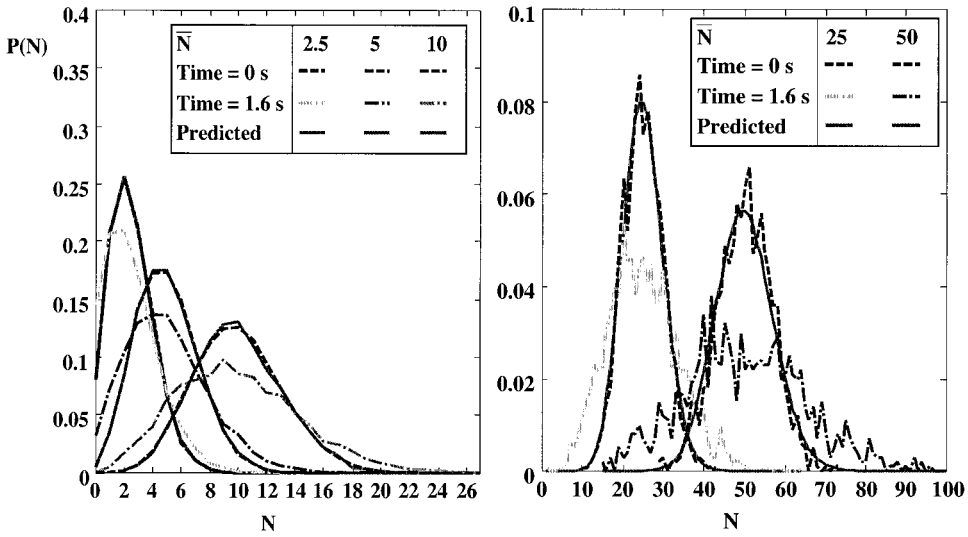

FIG. 7. Same as Fig. 1 for the comparison between a Poisson distribution (solid line) and the virtual sampling of the PV droplet fields. The dashed lines labeled 0 s in the legend correspond to the initial random field; the dot–dashed line labeled 1.6 s corresponds to the field after 1.6 s of simulation.

coupling progressively generates preferential concentration. The $F(L)$ values increase from a few units for the initial field, to values between 50 and 100 for the final one. This test confirms the conclusions of the counting statistics. The $F(L)$ values for the actual fields shown in Fig. 3 are lower than ± 3 within the range of scales from 1 to 10 cm. This is closer to the PV initial field properties than to the properties of the following fields, even at $t = 0.16$ s, where $F(L)$ reaches values of the order of 20. Scales larger than 2 cm are not documented with the simulation because the model domain is limited to 1 dm^3.

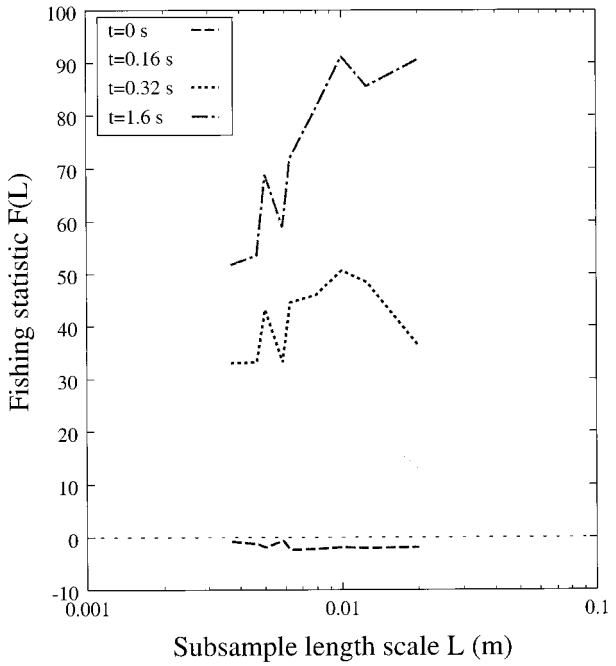

FIG. 8. Same as Fig. 3b for the PV droplet fields, at various time steps of the simulation, as indicated in the legend.

In Fig. 9 the counting statistics of the RS simulation are compared to the Poisson reference and to distributions derived from the same actual droplet spatial distribution as in Fig. 6. The RS simulation is characterized by a mean droplet number concentration of $\overline{C} = 260$ cm^{-3}, while $\overline{C} = 225$ cm^{-3} in the actual sample shown in Fig. 6. Subsample volumes have thus been selected so that the expected number of counts $\overline{N}$ in both cases are similar, from about 5 (Fig. 9a) to about 50 (Fig. 9d), that is, subsample volumes from 0.02 to 0.2 cm^{-3}. The RS simulation exhibits an exponential trend strongly contrasting with both the Poisson reference and the actual sample. This is confirmed in Fig. 10 by the Fishing test with $F(L)$ values from 1600 at a length scale of 3 mm to 3000 at the centimeter scale, while the values in actual samples are lower than 10 at any scale, from 2 mm to 10 m.

b. Discussion

The two modeling studies of Vaillancourt (1998) and Shaw et al. (1998) are particularly interesting in the context of droplet inertial coupling and its effects on DSB, because they reach opposite conclusions. Vaillancourt's study is based on explicit simulation of individual droplet growth in a 3D DNS field, including inertial coupling and droplet sedimentation. It is however limited to Reynolds numbers smaller than in actual clouds and it cannot resolve heat and water vapor diffusion at the smallest scale. The main conclusion is that inertial coupling does not contribute significantly to DSB. The approach in Shaw et al. is rather based on a conceptual

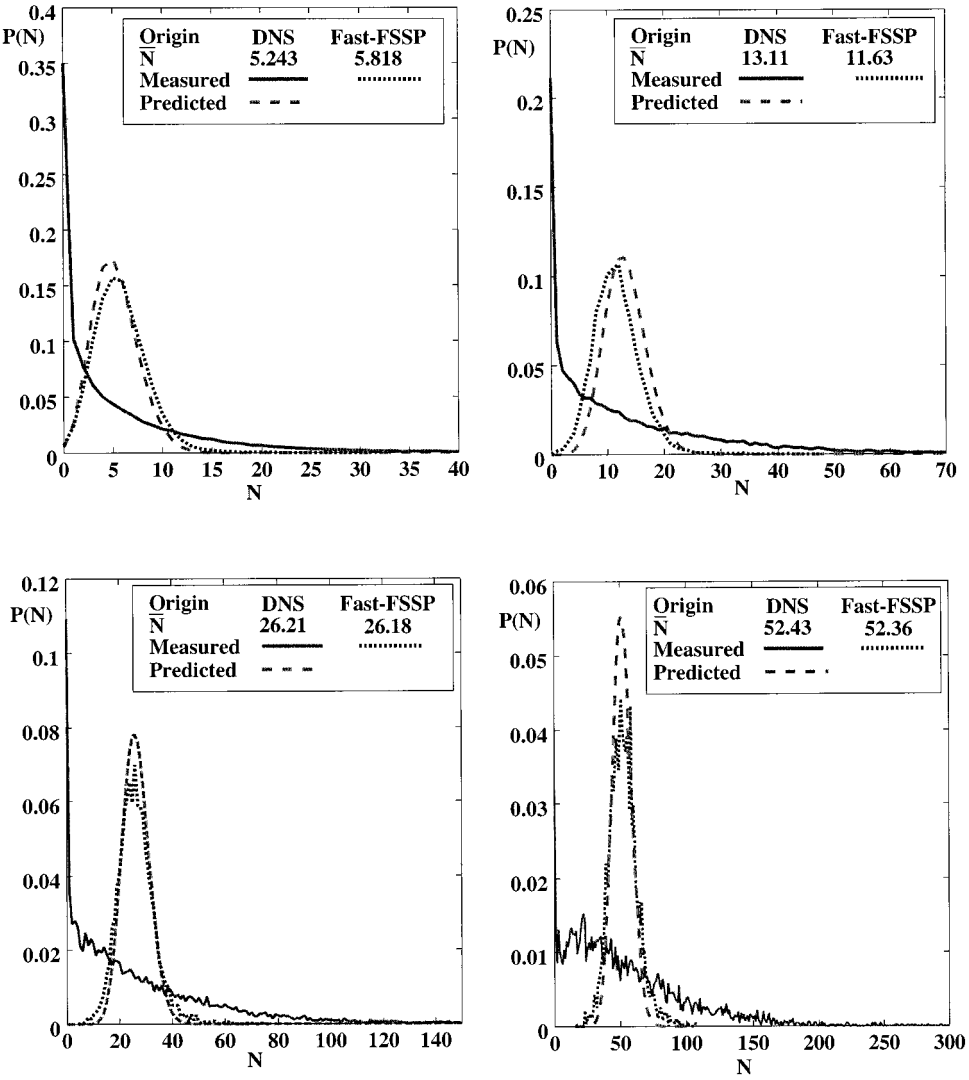

FIG. 9. Same as Fig. 1 for the comparison between a Poisson distribution (dashed lines), the distribution derived from the actual sample shown in Fig. 6 (dot–dashed lines), and the virtual sampling of the RS droplet field (solid lines), for various values of $\overline{N}$, as indicated in the legend.

model, where the flow was assumed to contain intense, relatively long-lived vortices. The conclusion is that inertial coupling significantly broadens droplet spectra. The purpose here is not to compare and evaluate the two approaches, whose limitations are already discussed in Grabowski and Vaillancourt (1999) and Shaw et al. (1999). These short notes suggest that the numerical approach is far from providing definite answers because of computer-limited performances.

Our point is that the experimental approach should help in the meantime for the selection of the most realistic hypotheses and rejection of unrealistic concepts. In the conceptual model of Shaw et al. (1998), the main features are the hypothesis that small-scale vortices in the atmosphere occupy a large fraction of the cloud volume, that their lifetime is much longer than the vortex turnover time and Kolmogorov timescale, and that it rather scales with the integral timescale. Parameters such as the lifetime of the turbulent structures cannot be documented with in situ airborne measurements that always provide an instantaneous picture of cloud microphysics. However, if fluctuations of the droplet concentration by a factor of 10 between the minimum and the maximum values (Fig. 4 in Shaw et al.), with a typical length scale of a centimeter, were filling the cloud volume, as assumed in Shaw et al., they would obviously be noticeable in the counting statistics or the Fishing test.

The regions selected here, as the regions of narrowest spectra, are also characterized by the lowest values of the turbulent eddy dissipation rate and of the droplet concentration heterogeneity, as measured with counting

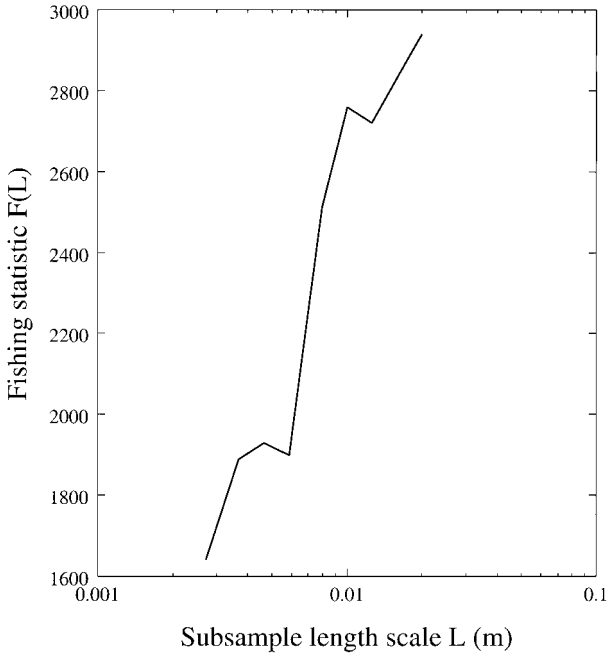

FIG. 10. Same as Fig. 3b for the RS droplet field.

statistics or the Fishing test. It is difficult to estimate the eddy dissipation rate on cloud samples as short as a few hundreds of meters from airborne measurements of the air vertical velocity, which are limited to a spatial resolution of 4 m. However an evaluation obtained by spectral analysis of all the selected samples combined suggests values as small as $\epsilon = 1$–10 cm^2 s^{-3}, while ϵ reaches values between 100 and 1000 cm^2 s^{-3} in the entraining regions of the cloud. Shaw et al. consider that preferential concentration becomes significant at $\epsilon = 100$ cm^2 s^{-3}. However, even in cloud regions with such values of the turbulent eddy dissipation rate, the counting statistics never show deviations as large as a factor of 10 apart of the mean value.

It is still possible that inertial coupling of the droplets with turbulent vortices could play a role in the most turbulent entraining regions. Unfortunately, these regions are also strongly affected by mixing with the environmental dry air that generates concentration heterogeneities down to the very small mm scale. It is therefore impossible to distinguish between evaporation and inertial effects from only the analysis of the droplet spatial distribution. The next step will be to focus the experimental analysis on regions dynamically active but not significantly affected by the mixing with dry air. This will be discussed in Part III of the series.

These observations do not validate or invalidate the conclusions of the models. However, they clearly demonstrate that simulations such as shown in Fig. 1 of Shaw et al. (1998) do not illustrate realistically the preferential concentration in convective clouds.

In Part I of this series, quasi-adiabatic cloud samples of narrow spectra have been examined up to altitudes of more than 1500 m above cloud base. The observed spectra are broader than predicted by the adiabatic model of convective lifting and droplet condensational growth. In particular they show proportions of both small and big droplets larger than in the adiabatic reference. The presence of small droplets can be accounted for by assuming CCN secondary activation and some contribution of the mixing processes. The large proportions of big droplets are likely to be instrumental artifacts due to droplet coincidences in the detection beam of the instrument (section 4 in Part I). The core of the observed spectra is however still broader than the adiabatic reference. The objective here is to document concentration heterogeneities at the microscale to evaluate if they could explain that broadening. Counting statistics and the Fishing test both converge in showing that concentration heterogeneities are not significant. Statistical properties remain close to the Poisson reference, within the range of uncertainty due to the limited number of samples. Preferential concentration is not supported by the observations made in convective cores, either because the turbulent eddy dissipation rate is too low or because coherent vortices occupy a much smaller volume than assumed in Shaw et al. (1998).

Conceptual models shall thus be revised by showing how coherent vortices can remain undetectable by counting statistics and the Fishing test, yet significantly contributing to spectra broadening.

7. Conclusions

The samples of narrow spectra selected in Part I for the characterization of DSB in unmixed cloud samples have been further analyzed here to document the statistical properties of the droplet spatial distribution. It has been shown that the counting statistics and the Fishing test do not deviate significantly from the Poisson reference, which characterizes a random spatial distribution of droplets. A conceptual model of DSB has been developed to evaluate the effect on DSB of the observed heterogeneities. The conceptual model suggests that they could be responsible for the observed DSB, only if their lifetime reached unrealistically long values.

However, in situ data do not provide information about the time evolution of the droplet fields, and the conceptual model fails at reproducing the main processes involved in that time evolution. One can thus raise the question of the sensitivity of the statistical tests used here for evaluating the effect of concentration heterogeneities on DSB.

DNS models, with explicit calculations of heat and vapor diffusion, and droplet growth have been recently developed to simulate the effects of droplet inertia on heterogeneities of the droplet concentration. Two simulations have been considered here: the Vaillancourt's DNS model and a simulation provided by Shaw to illustrate preferential concentration. The same statistical tests, counting statistics and Fishing test, have been per-

formed on the simulated fields. Both simulations deviate more from the Poisson prediction than the actual data do. In fact the simulated droplet field that is the most comparable with the observations is the initial field in the PV simulation, where droplets are randomly distributed. The observations do not support either the conceptual description of droplet concentration heterogeneities as suggested by Shaw et al.

Our conclusion is thus that the concentration heterogeneities observed in adiabatic cores are not sufficient to support the concept of preferential concentration. In particular the values of eddy dissipation rate measured in adiabatic cores are lower than the minimum value indicated by Shaw et al. for generating preferential concentration. Regions of much higher turbulent eddy dissipation rates are observed but they are also strongly affected by droplet evaporation following mixing with the environmental air, which prevents the experimental identification of preferential concentration. The next step will be to focus the experimental analysis on regions that are dynamically active but not significantly affected by mixing processes with dry air. This will be discussed in Part III of the series. As far as future numerical approaches are concerned, it will be crucial to predict features of the droplet fields that can be verified with in situ measurements.

Acknowledgments. The authors acknowledge the support of Météo-France, the National Center for Atmospheric Research, Department of Atmospheric Sciences at the University of Wyoming, INSU under Grant 95317, and the European Commission under Grant ENV4*CT950117. P. Vaillancourt and R. Shaw are particularly acknowledged for providing the simulated fields and for their very constructive comments for improving the manuscript.

REFERENCES

Baker, B., 1992: Turbulent entrainment and mixing in clouds: A new observational approach. *J. Atmos. Sci.,* **49,** 387–404.

Barlow, R. J., 1989: *Statistics: A Guide to the Use of Statistical Methods in the Physical Sciences*. John Wiley and Sons, 222 pp.

Brenguier, J. L., 1993: Observations of cloud microstructure at the centimeter scale. *J. Appl. Meteor.,* **32,** 783–793.

——, and L. Chaumat, 2001: Droplet spectra broadening in cumulus clouds. Part I: Broadening in adiabatic cores. *J. Atmos. Sci.,* **58,** 628–641.

——, T. Bourrianne, A. A. Coelho, J. Isbert, R. Peytavi, D. Trevarin, and P. Wechsler, 1998: Improvements of the droplet size distribution measurements with the Fast-FSSP. *J. Atmos. Oceanic Technol.,* **15,** 1077–1090.

Cooper, W. A., 1989: Effects of variable droplet growth histories on droplet size distributions. Part. I: Theory. *J. Atmos. Sci.,* **46,** 1301–1311.

Grabowski, W. W., and P. Vaillancourt, 1999: Comments on ''Preferential concentration of cloud droplets by turbulence: Effects on the early evolution of cumulus cloud droplet spectra.'' *J. Atmos. Sci.,* **56,** 1433–1436.

Pawlowska, H., J. L. Brenguier, and G. Salut, 1997: Optimal nonlinear estimation for cloud particle measurements. *J. Atmos. Oceanic Technol.,* **14,** 88–104.

Shaw, R. A., W. C. Reade, L. R. Collins, and J. Verlinde, 1998: Preferential concentration of cloud droplets by turbulence: Effects on the early evolution of cumulus cloud droplet spectra. *J. Atmos. Sci.,* **55,** 1965–1976.

——, ——, ——, and ——, 1999: Reply. *J. Atmos. Sci.,* **56,** 1437–1441.

Snyder, D. L., 1975: *Random Point Processes*. John Wiley and Sons, 495 pp.

Squires, P., 1952: The growth of cloud drops by condensation. *Aust. J. Sci. Res.,* **5,** 66–86.

Srivastava, R. C., 1989: Growth of cloud drops by condensation: A criticism of currently accepted theory and a new approach. *J. Atmos. Sci.,* **46,** 869–887.

Vaillancourt, P. A., 1998: Microscopic approach to cloud droplet growth by condensation. Ph.D. dissertation, McGill University, 154 pp. [Available from Canadian Theses Service, Acquisitions and Bibliographic Services, National Library of Canada, 395 Wellington Street, Ottawa K1A ON4, Canada.]

——, and M. K. Yau, 2000: Review of particle-turbulence interactions and consequences for cloud physics. *Bull. Amer. Meteor. Soc.,* **81,** 285–298.

——, M. K. Yau, and W. W. Grabowski, 1998: Micropscopic approach to cloud droplet growth by condensation. Preprints, *Conf. on Cloud Physics,* Everett, WA, Amer. Meteor. Soc., 546–549.

——, ——, and ——, 2001: Microscopic approach to cloud droplet growth by condensation. Part I: Model description and results without turbulence. *J. Atmos. Sci.,* in press.